Research Article | Vol. 7, No. 10 | 1 Oct 2016 | BIOMEDICAL OPTICS EXPRESS 4125
Biomedical Optics EXPRESS

Biodegradable polymeric nanoparticles containing gold nanoparticles and Paclitaxel for cancer imaging and drug delivery using photoacoustic methods

YANJIE WANG,[1,2,3] ERIC M. STROHM,[1,2,3] YANG SUN,[4] ZHAOXIA WANG,[5] YUANYI ZHENG,[6] ZHIGANG WANG,[4] AND MICHAEL C. KOLIOS[1,2,3,*]

[1]*Physics Department, Ryerson University, 350 Victoria St., Toronto, Ontario M5B 2K3, Canada*
[2]*Institute for Biomedical Engineering, Science and Technology (iBEST), a partnership between Ryerson University and St. Michael's Hospital, 30 Bond St., Toronto, Ontario, M5B 1T8, Canada*
[3]*Keenan Research Centre for Biomedical Science of St. Michael's Hospital, 30 Bond St., Toronto, Ontario, M5B 1T8, Canada*
[4]*Institute of Ultrasound Imaging, Second Affiliated Hospital, Chongqing Medical University, 76 Linjiang Rd., Chongqing, 400010, China*
[5]*Department of Ultrasound, Children's Hospital, Affiliated to Chongqing Medical University, No.136, Zhongshan No.2 Rd., Yuzhong District, Chongqing 400014, China*
[6]*Ultrasound Department, Sixth affiliated hospital of Shanghai Jiaotong University, 600 Yishan Rd., Xuhui District, Shanghai, 200133, China*
[*]*mkolios@ryerson.ca*

Abstract: In this study, optical-triggered multifunctional theranostic agents for photoacoustic/fluorescent imaging and cancer therapy have been developed. This system consists of a perfluorohexane liquid and gold nanoparticles (GNPs) in the core, stabilized by a Poly (lactide-co-glycolic acid) (PLGA) polymer shell. When cancer cells containing PLGA-GNPs were exposed to laser pulses, cell viability decreased due to the vaporization of the particles in and around the cells. The particle chemo drug loading and delivery capacity was also investigated in vitro experiments. These particles show potential as photoacoustic imaging and therapy agents for future clinical translation in cancer therapy.

OCIS codes: (160.4236) Nanomaterials; (160.1435) Biomaterials; (170.5120) Photoacoustic imaging; (170.3880) Medical and biological imaging; (170.2520) Fluorescence microscopy.

References and links

1. X. Wang, Y. Wang, Z. G. Chen, and D. M. Shin, "Advances of Cancer Therapy by Nanotechnology," Cancer Res. Treat. **41**(1), 1–11 (2009).
2. R. Duncan, "Polymer conjugates as anticancer nanomedicines," Nat. Rev. Cancer **6**(9), 688–701 (2006).
3. I. Brigger, C. Dubernet, and P. Couvreur, "Nanoparticles in cancer therapy and diagnosis," Adv. Drug Deliv. Rev. **54**(5), 631–651 (2002).
4. J. Panyam and V. Labhasetwar, "Biodegradable nanoparticles for drug and gene delivery to cells and tissue," Adv. Drug Deliv. Rev. **55**(3), 329–347 (2003).
5. S. K. Sahoo and V. Labhasetwar, "Nanotech approaches to drug delivery and imaging," Drug Discov. Today **8**(24), 1112–1120 (2003).
6. A. Kumari, S. K. Yadav, and S. C. Yadav, "Biodegradable polymeric nanoparticles based drug delivery systems," Colloids Surf. B Biointerfaces **75**(1), 1–18 (2010).
7. J. Liu, J. Li, T. J. Rosol, X. Pan, and J. L. Voorhees, "Biodegradable nanoparticles for targeted ultrasound imaging of breast cancer cells in vitro," Phys. Med. Biol. **52**(16), 4739–4747 (2007).
8. P. Kocbek, N. Obermajer, M. Cegnar, J. Kos, and J. Kristl, "Targeting cancer cells using PLGA nanoparticles surface modified with monoclonal antibody," J. Control. Release **120**(1-2), 18–26 (2007).
9. A. Lamprecht, N. Ubrich, H. Yamamoto, U. Schäfer, H. Takeuchi, P. Maincent, Y. Kawashima, and C.-M. Lehr, "Biodegradable nanoparticles for targeted drug delivery in treatment of inflammatory bowel disease," J. Pharmacol. Exp. Ther. **299**(2), 775–781 (2001).
10. J. Panyam and V. Labhasetwar, "Sustained Cytoplasmic Delivery of Drugs with Intracellular Receptors Using Biodegradable Nanoparticles," Mol. Pharm. **1**(1), 77–84 (2004).

#272474 http://dx.doi.org/10.1364/BOE.7.004125
Journal © 2016 Received 1 Aug 2016; revised 8 Sep 2016; accepted 13 Sep 2016; published 16 Sep 2016

Biomedical Optics EXPRESS

11. J. M. Koziara, T. R. Whisman, M. T. Tseng, and R. J. Mumper, "In-vivo efficacy of novel paclitaxel nanoparticles in paclitaxel-resistant human colorectal tumors," J. Control. Release **112**(3), 312–319 (2006).
12. A. A. Oraevsky, S. L. Jacques, and F. K. Tittel, "Determination of tissue optical properties by piezoelectric detection of laser-induced stress waves," in *Proceedings of Optics, Electro-Optics, & Laser Applications in Science& Engineering*, (International Society for Optics and Photonics,1993), pp. 86–101.
13. E. Hysi, E. M. Strohm, and M. C. Kolios, "Probing Different Biological Length Scales Using Photoacoustics: From 1 To 1000 MHz," in *Handbook of Photonics for Biomedical Engineering*, A. H.-P. Ho, D. Kim, and M. G. Somekh, Eds. (Springer, 2014).
14. M. Xu and L. V. Wang, "Photoacoustic imaging in biomedicine," Rev. Sci. Instrum. **77**(4), 041101 (2006).
15. P. Beard, "Biomedical photoacoustic imaging," Interface Focus **1**(4), 602–631 (2011).
16. P. Carmeliet and R. K. Jain, "Angiogenesis in cancer and other diseases," Nature **407**(6801), 249–257 (2000).
17. A. Roggan, M. Friebel, K. Do Rschel, A. Hahn, and G. Mu Ller, "Optical properties of circulating human blood in the wavelength range 400–2500 nm," J. Biomed. Opt. **4**(1), 36–46 (1999).
18. R. Weissleder, "A clearer vision for in vivo imaging," Nat. Biotechnol. **19**(4), 316–317 (2001).
19. A. A. Oraevsky, A. A. Karabutov, and E. V. Savateeva, "Enhancement of optoacoustic tissue contrast with absorbing nanoparticles," in *Proceedings of European Conference on Biomedical Optics*, (International Society for Optics and Photonics, 2001), pp. 60–69.
20. C. Kim, E. C. Cho, J. Chen, K. H. Song, L. Au, C. Favazza, Q. Zhang, C. M. Cobley, F. Gao, Y. Xia, and L. V. Wang, "In Vivo Molecular Photoacoustic Tomography of Melanomas Targeted by Bioconjugated Gold Nanocages," ACS Nano **4**(8), 4559–4564 (2010).
21. J. A. Copland, M. Eghtedari, V. L. Popov, N. Kotov, N. Mamedova, M. Motamedi, and A. A. Oraevsky, "Bioconjugated gold nanoparticles as a molecular based contrast agent: implications for imaging of deep tumors using optoacoustic tomography," Mol. Imaging Biol. **6**(5), 341–349 (2004).
22. J. P. Culver, R. Choe, M. J. Holboke, L. Zubkov, T. Durduran, A. Slemp, V. Ntziachristos, B. Chance, and A. G. Yodh, "Three-dimensional diffuse optical tomography in the parallel plane transmission geometry: evaluation of a hybrid frequency domain/continuous wave clinical system for breast imaging," Med. Phys. **30**(2), 235–247 (2003).
23. Y. Sun, Y. Wang, C. Niu, E. M. Strohm, Y. Zheng, H. Ran, R. Huang, D. Zhou, Y. Gong, Z. Wang, D. Wang, and M. C. Kolios, "Laser-Activatible PLGA Microparticles for Image-Guided Cancer Therapy In Vivo," Adv. Funct. Mater. **24**(48), 7674–7680 (2014).
24. J. G. Riess, "Perfluorocarbon-based oxygen delivery," Artif. Cells Blood Substit. Immobil. Biotechnol. **34**(6), 567–580 (2006).
25. O. D. Kripfgans, J. B. Fowlkes, D. L. Miller, O. P. Eldevik, and P. L. Carson, "Acoustic droplet vaporization for therapeutic and diagnostic applications," Ultrasound Med. Biol. **26**(7), 1177–1189 (2000).
26. R. E. Apfel, "Activatable infusable dispersions containing drops of a superheated liquid for methods of therapy and diagnosis," US5840276 A (1998).
27. P. S. Sheeran, S. Luois, P. A. Dayton, and T. O. Matsunaga, "Formulation and Acoustic Studies of a New Phase-Shift Agent for Diagnostic and Therapeutic Ultrasound," Langmuir **27**(17), 10412–10420 (2011).
28. E. Strohm, M. Rui, I. Gorelikov, N. Matsuura, and M. Kolios, "Vaporization of perfluorocarbon droplets using optical irradiation," Biomed. Opt. Express **2**(6), 1432–1442 (2011).
29. K. Wilson, K. Homan, and S. Emelianov, "Biomedical photoacoustics beyond thermal expansion using triggered nanodroplet vaporization for contrast-enhanced imaging," Nat. Commun. **3**, 618 (2012).
30. W. Cui, J. Bei, S. Wang, G. Zhi, Y. Zhao, X. Zhou, H. Zhang, and Y. Xu, "Preparation and evaluation of poly(L-lactide-co-glycolide) (PLGA) microbubbles as a contrast agent for myocardial contrast echocardiography," J. Biomed. Mater. Res. B Appl. Biomater. **73B**(1), 171–178 (2005).
31. E. Pisani, N. Tsapis, J. Paris, V. Nicolas, L. Cattel, and E. Fattal, "Polymeric Nano/Microcapsules of Liquid Perfluorocarbons for Ultrasonic Imaging: Physical Characterization," Langmuir **22**(9), 4397–4402 (2006).
32. K. E. Uhrich, S. M. Cannizzaro, R. S. Langer, and K. M. Shakesheff, "Polymeric systems for controlled drug release," Chem. Rev. **99**(11), 3181–3198 (1999).
33. M. L. Fabiilli, J. A. Lee, O. D. Kripfgans, P. L. Carson, and J. B. Fowlkes, "Delivery of Water-Soluble Drugs Using Acoustically Triggered Perfluorocarbon Double Emulsions," Pharm. Res. **27**(12), 2753–2765 (2010).
34. J. Spratlin and M. B. Sawyer, "Pharmacogenetics of paclitaxel metabolism," Crit. Rev. Oncol. Hematol. **61**(3), 222–229 (2007).
35. M. Ishitobi, E. Shin, and N. Kikkawa, "Metastatic breast cancer with resistance to both anthracycline and docetaxel successfully treated with weekly paclitaxel," Int. J. Clin. Oncol. **6**(1), 55–58 (2001).
36. M. Yokoyama, M. Miyauchi, N. Yamada, T. Okano, Y. Sakurai, K. Kataoka, and S. Inoue, "Characterization and anticancer activity of the micelle-forming polymeric anticancer drug adriamycin-conjugated poly(ethylene glycol)-poly(aspartic acid) block copolymer," Cancer Res. **50**(6), 1693–1700 (1990).
37. M. Talelli, C. J. F. Rijcken, W. E. Hennink, and T. Lammers, "Polymeric micelles for cancer therapy: 3 C's to enhance efficacy," Curr. Opin. Solid State Mater. Sci. **16**(6), 302–309 (2012).
38. J. Turkevich, P. C. Stevenson, and J. Hillier, "A study of the nucleation and growth processes in the synthesis of colloidal gold," Discuss. Faraday Soc. **11**(0), 55–75 (1951).
39. G. Frens, "Particle size and sol stability in metal colloids," Kolloid-Z. Z. Für Polym. **250**(7), 736–741 (1972).

Biomedical Optics EXPRESS

40. N. G. Bastús, J. Comenge, and V. Puntes, "Kinetically Controlled Seeded Growth Synthesis of Citrate-Stabilized Gold Nanoparticles of up to 200 nm: Size Focusing Versus Ostwald Ripening," Langmuir **27**(17), 11098–11105 (2011).
41. S. H. Liu and M. Y. Han, "Synthesis, Functionalization, and Bioconjugation of Monodisperse, Silica-Coated Gold Nanoparticles: Robust Bioprobes," Adv. Funct. Mater. **15**(6), 961–967 (2005).
42. I. Gorelikov, A. L. Martin, M. Seo, and N. Matsuura, "Silica-coated quantum dots for optical evaluation of perfluorocarbon droplet interactions with cells," Langmuir **27**(24), 15024–15033 (2011).
43. Y. J. Wang, E. M. Strohm, Y. Sun, C. Niu, Y. Zheng, Z. Wang, and M. C. Kolios, "PLGA/PFC particles loaded with gold nanoparticles as dual contrast agents for photoacoustic and ultrasound imaging," Proc. SPIE **8943**, 89433M (2014).
44. S. L. Lombardi, ed., *Nanoparticles: new research*, (Nova Science Publishers, 2008).
45. Y.-S. Chen, W. Frey, S. Kim, P. Kruizinga, K. Homan, and S. Emelianov, "Silica-Coated Gold Nanorods as Photoacoustic Signal Nanoamplifiers," Nano Lett. **11**(2), 348–354 (2011).
46. Y. Matsumura and H. Maeda, "A New Concept for Macromolecular Therapeutics in Cancer Chemotherapy: Mechanism of Tumoritropic Accumulation of Proteins and the Antitumor Agent Smancs," Cancer Res. **46**(12 Pt 1), 6387–6392 (1986).
47. F. Yuan, M. Dellian, D. Fukumura, M. Leunig, D. A. Berk, V. P. Torchilin, and R. K. Jain, "Vascular Permeability in a Human Tumor Xenograft: Molecular Size Dependence and Cutoff Size," Cancer Res. **55**(17), 3752–3756 (1995).
48. C. L. Didychuk, P. Ephrat, A. Chamson-Reig, S. L. Jacques, and J. J. L. Carson, "Depth of photothermal conversion of gold nanorods embedded in a tissue-like phantom," Nanotechnology **20**(19), 195102 (2009).
49. C. W. Wei, M. Lombardo, K. Larson-Smith, I. Pelivanov, C. Perez, J. Xia, T. Matula, D. Pozzo, and M. O'Donnell, "Nonlinear contrast enhancement in photoacoustic molecular imaging with gold nanosphere encapsulated nanoemulsions," Appl. Phys. Lett. **104**(3), 033701 (2014).
50. A. J. Dixon, S. Hu, A. L. Klibanov, and J. A. Hossack, "Oscillatory Dynamics and In Vivo Photoacoustic Imaging Performance of Plasmonic Nanoparticle-Coated Microbubbles," Small **11**(25), 3066–3077 (2015).
51. J. L. Goldstein, R. G. W. Anderson, and M. S. Brown, "Coated pits, coated vesicles, and receptor-mediated endocytosis," Nature **279**(5715), 679–685 (1979).
52. D. B. Chithrani, "Intracellular uptake, transport, and processing of gold nanostructures," Mol. Membr. Biol. **27**(7), 299–311 (2010).

1. Introduction

Cancer remains as a deadly disease which affects millions of people around the world. Conventional chemotherapy often results in severe side effects due to the non-targeted drug delivery [1]. The outstanding progress in nanotechnology provides an alternative therapeutic strategy for treating cancer [2]. Over the past few decades, there has been considerable interest in developing biodegradable nanoparticles (NPs) as effective drug delivery devices [3, 4] due to their enhanced drug loading capacity, biological stability and sustainable circulation time in vivo [5,6]. These nano-particles have the ability of functional conjugation to facilitate targeting [7–9], and are able to deliver drugs at intracellular locations, thereby resulting in enhanced therapeutic action [3, 10, 11]. Although, many nano-systems have been developed for cancer diagnosis and therapy, most of them are designed for single or dual purposes. They lack of multifunctional capacities.

Tumor imaging plays a key role in clinical oncology by helping to identify solid tumors and monitor therapeutic responses. Photoacoustic (PA) imaging is a new non-invasive biomedical imaging modality combining the high contrast of optical imaging with the high resolution of ultrasound (US) imaging [12, 13]. When illuminated by a laser source, optical absorbing particles and structures emit a pressure wave with frequencies in the ultrasonic range called PA waves. In PA imaging the contrast is based on tissue optical absorption properties unlike an US image in which the contrast depends on tissue biomechanical properties. PA imaging is ideally suited for detecting light-absorbing chromophores in the tissue, typically providing greater specificity than conventional US imaging [14, 15].

Tumors can often be differentiated from normal tissues due to the increased angiogenesis inside the tumors [16]; the increased blood content can be detected using PA imaging [17]. However, in the early stage of cancer development, tumor imaging resolution is limited due to lack of contrast between cancer and surrounding normal tissues. Thus, exogenous chemical agents that can enhance the contrast between cancerous and normal tissues for early cancer diagnosis are widely used [18, 19]. Among them, plasmonic gold nanoparticles (GNPs) have

Biomedical Optics EXPRESS

been extensively investigated for imaging tumors [20, 21] due to their inert chemical properties and excellent optical absorbing capabilities in the visible to near infrared wavelength range where the absorption of tissues is a minimum [22].

In our previous study, we developed micro-particles as theranostic agents. They were containing a perfluorohexane (PFH) liquid stabilized by Poly (lactide-co-glycolic acid) (PLGA) shells, with GNPs incorporated in the shells as the optical absorbers for PA/US imaging [23]. Perfluorocarbon (PFC) liquids have long been used as blood substitutes to carry oxygen in patients due to their chemical and biological inert, and non-toxic properties [24]. Droplets made of low boiling temperature PFC undergo a phase transition when the liquid core vaporize to gaseous states when perturbed through sufficient acoustic pressures [25, 26] However, applications involving nano-sized droplet vaporization with relatively low ultrasound frequencies may require pressures significantly higher than diagnostic US machines currently provide, increasing the potential for unwanted bio-effects [27]. Vaporization can also be induced via laser irradiation with the facilitation of optical absorbers incorporated inside the droplets [28, 29] to avoid the potential damage to the tissue caused by high pressure US.

Nano-particles stabilized by biodegradable and biocompatible PLGA polymer shells have the advantages over other types of nanoparticles. They slowly degrade in vivo into lactic and glycolic acid. These can further degrade into carbon dioxide and water via the tricarboxylic acid cycle [30]. They are stable due to good mechanical strength than monomolecular layers of lipids or surfactants [30, 31]; they can also act as a good drug carrier or ligand for targeted imaging or targeted drug delivery [32, 33].

Our in vivo experiments indicate that laser-stimulated PLGA particle vaporization caused the disruption of the vasculature and decreased blood perfusion which caused necrosis of tumor cells, thus limiting tumor growth [23]. The anti-cancer therapeutic effects could be further enhanced by incorporating a chemotherapeutic into the particle. Paclitaxel (PAC) is a mitotic inhibitor that has high therapeutic efficacy against a range of solid tumors including breast cancer, advanced ovarian carcinoma, and lung cancer [34, 35]. However, its therapeutic effect in clinical applications is restricted due to its low solubility in solvents for intravascular injection. Many NPs carry drug through chemical covalent attachment to the NP surfaces which either result in premature drug release in the circulation, or create technically challenging and limiting their suitability for systemic drug delivery [36, 37].

Based on our previous work, in this study, we propose a method of combining an imaging and therapeutic technique in a single procedure by developing multifunctional nano-carriers (< 600 nm) for PA/fluorescent imaging and as drug delivery vehicles. In this design, GNPs were loaded in the core, and the water insoluble drug PAC and fluorescent dye was encapsulated into the PLGA shell. This formulation allows more GNPs encapsulated inside the PLGA particles and leaves more space in the PLGA shell for drug encapsulation. We tested the particle drug loading and delivery capacities in in vitro cell culture experiments, and demonstrated the effects of laser-induced particle vaporization on cell viability.

2. Materials and methods

2.1 Materials

All chemicals were at ACS grade and used without additional purification. Hydroauric acid ($HAuCl_4 \cdot 3H_2O$) (99%), Trisodium Citrate ($Na_3C_6H_5O_7$) (99%), Tetraethyl orthosilicate (TEOS), 1H,1H,2H,2H-perfluorodecyltriethoxysilane, Dichloromethane (CH_2Cl_2), PLGA (LA:GA 50:50), Perfluorohexane (C_6F_{14}), Paclitaxel, Fluorescent lipophilic carbocyanines dye DiI, DiO, Hoechst, and tetrazolium dye MTT 3-(4,5-dimethylthiazol-2-yl)-2,5-diphenyltetrazolium bromide were purchased from Sigma Aldrich Inc., Canada. Acetone, isopropanol, methanol, ammonia was purchased from Fisher Scientific Inc., Canada. Deionized water (Millipore Milli-Q grade) with resistivity of 18.2 MΩ was used in all experiments.

Biomedical Optics EXPRESS

2.2 PLGA particle synthesis

Gold nanospheres were synthesized based on the single-phase aqueous reduction of tetrachloauric acid by sodium citrate developed by Turkevich et al. [38] and Frens et al. [39], modified by Bastús et al. [40], then coated with silica according to a modified method described by Liu and Han [41], and fluorinated via 24 hour incubation at room temperature with 1H,1H,2H,2H-perfluorodecyltriethoxysilane [42]. After the solvent was evaporated, the fluorinated GNPs were dissolved into PFH liquid. PLGA particles containing PFH with and without GNPs were prepared using a double emulsion solvent evaporation process [23, 43]. Briefly, PLGA polymer (25 mg) and DiD or DiI (100 µg) were dissolved in dichloromethane (1 mL). GNPs in PFH solution (0.5 mL) was mixed with PLGA solution and was emulsified for 45 seconds, with 2-second-on, 1-second-off, 10 W pulses, using a tip sonifier (BRANSO, USA). Then the emulsion was homogenized with 6 mL, 4% polyvinyl alcohol solution for 30 seconds. The final emulsion was mixed with 2% isopropanol solution and stirred for 3 hours at room temperature to evaporate organic solvents and washed several times by centrifugation (5 minutes, 700 g). The final product were collected and stored at 4°C for future use. To load the therapeutic drug PAC into the PLGA particles, PAC (5 mg) was dissolved in the PLGA in dichloromethane solution, and then the double emulsion method was followed.

2.3 Paclitaxel drug loading efficiency

The amount of the encapsulated chemo drug in PLGA particles was determined using high-performance liquid chromatography (HPLC, Agilent, USA), equipped with a reversed phase Agilent Zorbax ODS C18 column (4.6 × 150 mm, particle size 5 µm). PLGA particles (2.5 mg) were dissolved in 1 mL acetonitrile to extract the encapsulated drug. The mobile phase consisted of an acetonitrile and water in the volumetric ratio of 50:50. The liquid flowrate of HPLC was 1 mL/min. The drug was detected using an UV detector. The absorbance of the drug was measured at wavelength of 250 nm at 8 minutes. Drug loading efficiency (LE) was determined as: LE% = (Mass_dect/Mass_theo)*100, where Mass_dect was the mass of drug detected by HPLC and Mass_theo was mass of drug expected in 2.5 mg of PLGA particles if the drug loading efficiency was 100%.

2.4 Photoacoustic measurements

The photoacoustic signals of PLGA-GNPs were measured using an acoustic/photoacoustic microscope (SASAM, Kibero GmbH, Germany) [28] which consists of an inverted optical microscope (IX81 Olympus, Japan), a 375 MHz transducer positioned above the sample stage and a 532 nm focused laser (Teem Photonics, France) collimated through the side port onto the sample. The laser had a 330 ps pulse width, 4 kHz repetition rate, and a maximum energy of 580 nJ per pulse when focused to a 10 µm spot. A drop of PLGA-GNPs water solution was deposited on top of a glass coverslip on the sample stage. A 10x objective was used to guide the alignment between laser and transducer foci. The PA signal amplitudes were measured while the laser energy was gradually increased. The process was repeated until vaporization occurred or the maximum laser energy level was reached. Three PLGA particle sizes (2, 5, and 10 µm in diameter) containing 14, 35, and 55 nm GNPs were measured. An average of ten measurements at each size was calculated for data analysis.

2.5 PLGA particle internalization by cancer cells

The human breast cancer MCF7 cells were purchased from American Type Culture Collection (ATCC) and maintained in a humidified cell incubator at 37 °C and 5% CO_2 with Dulbecco's Modified Eagle Media comprising 4500 mg glucose/L, L-glutamine, $NaHCO_3$, and sodium pyruvate with 10% fetal bovine serum, 1% HEPES buffer, and 1% penicillin-streptomycin. MCF7 cells were seeded at a concentration of 5×10^4 on a glass cover slip in a cell culture dish and incubated (37°C, 5% CO_2) for 12 hours. Then DiI labeled PLGA

Biomedical Optics EXPRESS

particles (50 µL, 250 µg/mL) loaded with 35 nm GNPs were added to the dish. After 5- and 20-hour incubation, the cells were washed with PBS (pH 7.4) to remove loosely attached and free particles in the medium. Next, the fluorescence dye DiO (40 µL, 8 µg/mL) was added in the media and left for 30-minute incubation. The fluorescent dye Hoechst (20 µL, 10 µg/mL) was added to the dish for 10 minutes. Finally, the cells were rinsed with PBS and fixed with 4% formaldehyde. After fixation, the cells were observed under a confocal laser scanning microscopy (LSM700, ZEISS, Germany) using a 20x objective. The confocal optical sections of cells at different depth were taken to investigate the PLGA-GNP internalization by cancer cells.

2.6 Photoacoustic and fluorescent imaging in vitro

Twenty thousand MCF7 cells were seeded in a 35 mm in diameter glass-bottom cell culture dish and incubated (37°C, 5% CO_2) for 12 hours. DiI labeled PLGA particles (50 µL, 375 µg/mL) loaded with 55 nm GNPs were added into the dish and incubated for 20 hours. The cells were washed with PBS (pH = 7.4) several times, and fluorescent dye Hoechst (40 µL, 10 µg/mL) and DiO (50 µL, 50 µg/mL) were added to the dish for 40 minutes. The cells were fixed with 4% formaldehyde. Then the cell culture dish was placed in the acoustic/photoacoustic microscope. PA c-scan images of MCF7 cells containing DiI labeled PLGA-GNPs particles were obtained with a 375 MHz transducer and a 532 nm laser with 5 µm spot size at fluence of 10 mJ/cm^2. The fluorescent and optical images were recorded prior to the PA imaging using a 20x objective. The fluorescent images were co-registered with the PA images and optical images.

2.7 Laser induced vaporization and drug release on cell viability

Initially, MCF7 cells were seeded in a glass-bottom 96-well plate (8000 cells per well) and left overnight in the incubator (37°C, 5% CO_2). PLGA-GNPs (100 µL, 375 µg/mL) and PLGA-PAC (100 µL, 75 µg PAC/mL) were added to each well according to the treatment and incubated for 6, 12 and 24 hours. GNPs of 35 nm in diameter were used for the PLGA-GNP synthesis. Then each well was rinsed with PBS (pH = 7.4). Cells treated with PLGA-GNPs were irradiated with a 532 nm pulsed laser (Minilite, Continuum, Canada) with a 3 ns pulse width, 10 Hz repetition rate, 100 mJ/cm^2 fluence, and 2 mm in diameter laser spot size for 5 seconds at each spots and 9 spots in each well in total. After all the treatments were completed, the cell viability was tested using MTT 3-(4,5-dimethylthiazol-2-yl)-2,5-diphenyltetrazolium bromide (MTT) assay.

3. Results and discussion

3.1 PLGA particle preparation and characterization

Three sizes of silica-coated GNPs were synthesized and encapsulated within the PLGA particles. Transmission electron microscopy (TEM) images (Fig. 1) show good mono-dispersity of silica-coated GNPs with gold core diameters of 13.9 ± 2.4, 34.9 ± 2.5 and 54.5 ± 4.2 nm with 20.0 ± 5.0 nm thick silica shells in aqueous solutions. The overall concentrations were $6.3x10^{12}$, $1.6x10^{11}$, and $4.6x10^{10}$ GNPs/ml of solution for 14, 35, and 55 nm GNPs, respectively, which were determined from atomic absorption spectroscopy (AAS) measurement.

Gold nanospheres were selected as the optical absorbing materials due to their high optical absorption, ease of synthesis, and small size permitting high-yield incorporation into nanometer sized PLGA particles. We used silica as a GNP coating agent since silica is chemically inert and optically transparent [44], and can enhances the PA signal strength and stabilizes GNPs under laser irradiation [45]. The silica shell also facilitated miscibilization of the GNPs into the hydrophobic and lipophobic PFH liquid using the ligand exchange

Biomedical Optics EXPRESS

technique [42]. PFH liquid has a boiling temperature around 56 °C. Particles made of PFH liquids are stable at physiological temperature prior to external stimuli.

The optical absorption and scattering spectra were measured and recorded using a Shimadzu spectrophotometer (Fig. 1). The absorption peaks of the 14, 35, and 55 nm GNPs were at 518, 528, and 536 nm, respectively. As the particle size increased, the absorption peaks demonstrates a red shift. The extinction coefficient amplitude is proportional to the optical absorption cross section of GNPs. The spectrum of 55 nm GNPs has a largest peak amplitude value comparing to the other two. For silica-coated GNPs, the spectral peaks are red shifted about 2 nm for 14 nm and 35 nm GNPs, and about 9 nm for 55 nm GNPs.

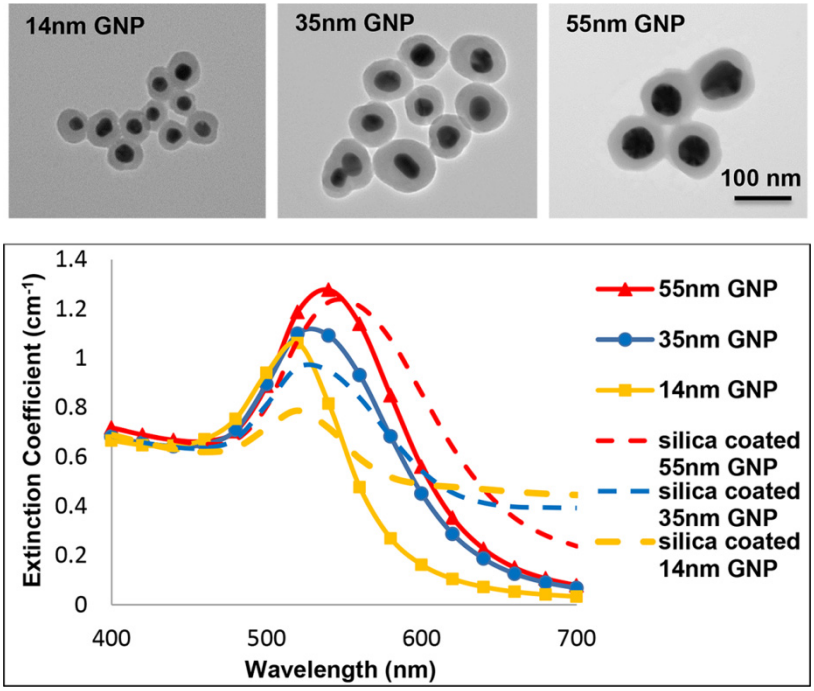

Fig. 1. (Top) TEM images of silica-coated GNPs, 14 nm, 35 nm, and 55 nm in diameter (dark areas) with silica shells (light gray areas). (Bottom) Optical extinction coefficients as function of wavelength are shown here in dashed yellow, blue and red lines, respectively. The extinction coefficient spectra of 14, 35 and 55 nm GNP solution are shown in solid yellow, blue and red lines. The scale bar is 100 nm for all figures.

PLGA particles were prepared via a water-oil-water double emulsion technique and characterized through several approaches. The structure of a single PLGA particle loaded with PFH liquid and silica-coated GNPs is schematically presented (Fig. 2(a)). TEM images of PLGA particles loaded with 14 nm, 35 nm and 55 nm GNPs are shown in Fig. 2(b)-2(d). The black dots are the GNPs and the gray background is the PLGA shell. Since the fluorinated silica-capped GNPs were well dispersed in the PFH liquid during the synthesis, most of them were located in the core with the PFH liquid. The GNPs are not uniformly distributed in the PLGA core, as shown in Fig. 2(c) and 2(d) due to the GNP aggregation. However, PLGA particles (large collections of GNPs) dominate the absorption and scattering; the small areas of the GNP aggregation did not affect the overall absorption spectra of PLGA-GNP particles.

Scanning electron microscopy (SEM) confirmed the spherical morphology of the PLGA particle (Fig. 2(e)). The PLGA shell thickness is about 10% of the particle diameter. The particle size range is from 0.486 to 9.25 μm with a mean size of 562 ± 91 nm (Fig. 2(f)) determined by laser diffraction technique using a Microtrac S3500 equipment (NIIKKISO

Biomedical Optics EXPRESS

Group, USA). In this study, the particle size distribution is rather large. For the future work, we will use membrane filters to screen out the larger size particles and keep the smaller ones (< 600 nm) for in vivo study since these size particles could pass through endothelial gaps in tumor vasculature much easier than the larger size particles due to the enhanced permeability and retention (EPR) effect [46, 47]. The absorption and scattering spectrum of a PLGA-GNP particle solution has a broad peak located around 530 nm in comparison with a spectrum of the GNP solution alone (Fig. 2(g)). This change is due to the scattering from the larger sizes of PLGA particles which is indicated by the spectrum of PLGA without GNPs.

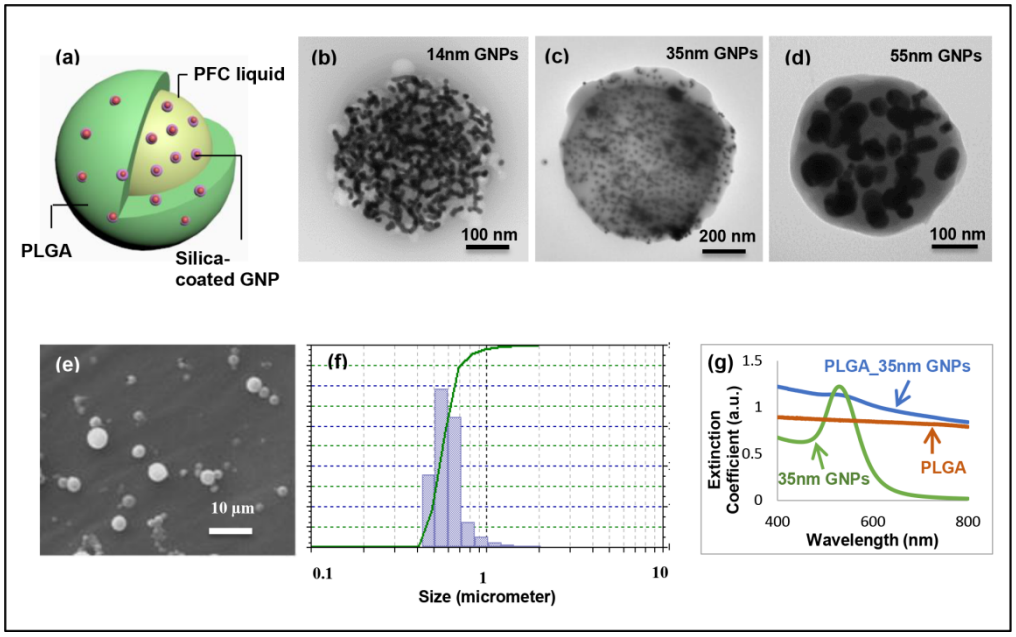

Fig. 2. (a) Schematic demonstration of the composition of a PLGA particle containing silica-coated gold nanoparticles and a PFH liquid. (b) – (d) TEM images of single PLGA particles loaded with PFH liquids and silica-coated GNPs. The black dots are the GNPs, and the gray pancake-shaped objects are the PLGA shells. (e) A SEM image of PLGA-GNP particles shows the spherical morphology. (f) The particle size distribution ranged from 0.486 to 9.25 μm with a mean size of 562 ± 91 nm. (g) Extinction coefficient as functions of laser wavelength for GNPs, PLGA particles and PLGA-GNP particles loaded with 35 nm GNPs.

3.2 Photoacoustic experiments in phantom study

The PA signals of micro-meter size PLGA-GNP particles were measured using a combined optical / acoustic microscope developed by Kibero, GmbH. The peak-to-peak photoacoustic signal amplitudes were used for the calculation of the PA signal intensity as functions of laser fluence and particle size. At low laser fluence level (<40 mJ/cm^2), the PA signal amplitudes increase linearly with the laser fluence (Fig. 3). The slope of each plot is also correlated with the particle size, and it is proportional to the GNP absorption coefficient. The larger GNPs with greater absorption cross section had a steeper slope than the smaller GNPs. Our results show that the 2 μm PLGA particles loaded with 55 nm, 35nm, and 14 nm GNPs produced lines with slopes of 0.141, 0.064, and 0.055 cm^{-1}, respectively (Fig. 3(a)). Larger PLGA particles encapsulating more GNPs result in stronger PA signals than the smaller particles. At higher fluence (>160 mJ/cm^2), the signal intensity levels off, potentially due to the deformation of the GNPs at high laser intensities [48]. Each dot in the graph is an average value of 10 independent measurements of individual PLGA particles of a specific size (Fig. 3(b), 3(c) and 3(d)).

Biomedical Optics EXPRESS

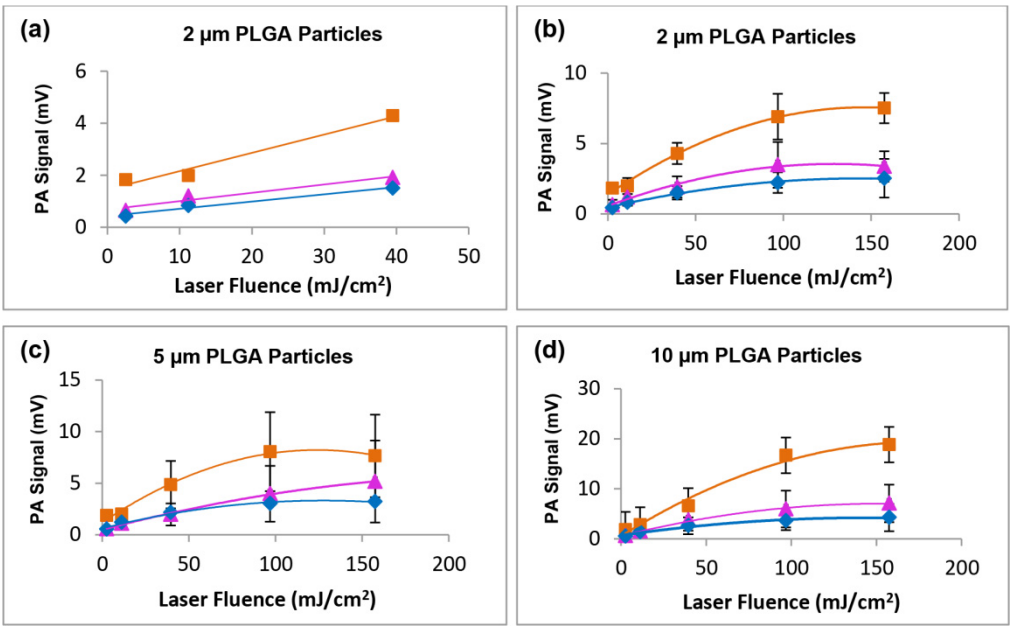

Fig. 3. (b)(c)(d) The PA signal as function of the laser fluence for three particle sizes are shown here. At the low energy level (<40mJ/cm^2), the PA signal is linearly proportional to the laser fluence for three types of PLGA particles (2, 5, and 10 µm). (a) The slope (0.141, 0.064, and 0.055 cm^{-1}) obtained from 2 µm PLGA-GNP particles is proportional to the GNP size, 55 nm, 35 nm, and 14 nm. In each graph, orange squares represent 55 nm GNPs, pink triangles represent 35 nm GNPs, and blue diamonds represent 14 nm GNPs. Error bars represent the standard deviation of ten measurements of one size of the PLGA particles.

The PLGA particle vaporization processes were recorded as video sequences (Fig. 4), in which the bubbles were formed instantaneously after the laser pulse irradiation, then expanded to approximately 10x the original particle size 2 seconds after vaporization. Then the bubble diameters slowly increased over time. The vaporization thresholds as functions of laser fluence were plotted in Fig. 4(b). Ten particles were measured for each type of PLGA-GNP particle. The vaporization threshold was defined as the point at which 50% (5 out of 10) or more of selected particles vaporized. The circles indicate the position where vaporization occurred, which was 170, 142 and 84 mJ/cm^2 for 5 µm PLGA-GNP particles loaded with 14, 35, and 55 nm GNPs, respectively. A lower fluence level was required for PLGA particles with larger GNPs and larger PLGA particles due to the larger absorption cross section of GNPs and greater amount of GNPs encapsulated in the PLGA particles.

The vaporization fluence threshold was higher compared to the published results in the literature, for example, fluence of 3.5 mJ/cm^2 demonstrated by Wei et al. [49]. There are a couple of reasons which may cause the differences. Firstly, our experiment was conducted on diluted samples. The vaporization threshold was based on the single particle vaporization without the thermal coupling from neighboring particles. In Wei's experiment, the vaporization was occurring with high concentration of nano-emulsions in a tube. The thermal coupling between closely packed gold nanospheres would reduce the laser fluence needed for the vaporization to occur. Secondly, the solid PLGA polymer shell could also make the vaporization more difficult to occur and therefore require more energy. The threshold fluence can be optimized in the future work by adjusting the GNP concentration and shell properties.

Biomedical Optics EXPRESS

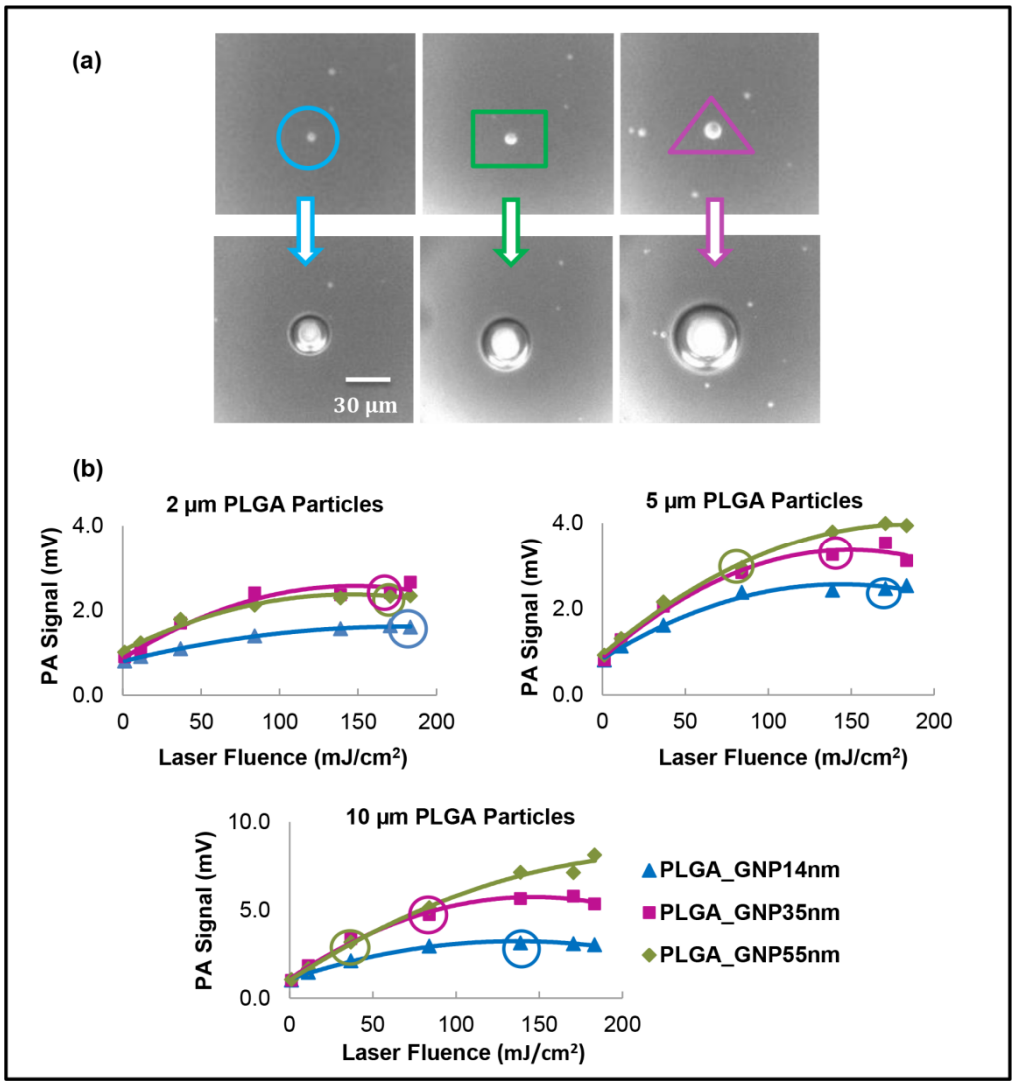

Fig. 4. (a) Optical images of PLGA-GNPs before and after vaporization. The initial particle diameter was 2, 5 and 10 µm (top row from left to right). The bubble diameter slowly increased to 20, 35, and 50 µm respectively after 2 seconds (bottom row from left to right). The scale bar is 30 µm for all images. (b) Photoacoustic signal amplitudes and vaporization threshold as functions of laser fluence and GNP sizes. The circle positions indicate when more than 50% of the particles vaporized.

During the vaporization threshold measurement, we observed that at the moment of the bubble formation, there were sudden large increases of the PA signals from the particles due to the vaporization event. This phenomenon was also reported in the literature [29, 49, 50]. After the bubbles formed, they grew about 10x of their original size in 2 seconds, then slowly grew with time to about 20x of their original size and were then stable for a couple of hours. The PA signals gradually decreased to the noise level as the bubbles gradually increased in size. This is because of the change in spacing of the GNPs on, or close to, the bubble surface. In previous experiments, we have determined that our focused transducer could not detect signal generated by a single GNP. For the future in vivo experiments, the bubbles and the GNPs would be confined in a tumor. Using an array transducer with a larger focus spot, the

Biomedical Optics EXPRESS

PA signals from the GNPs could be detected. In addition, any existing bubbles formed could be potential US contrast agents.

3.3 Internalization of PLGA particles by cancer cells

The PLGA-GNP particle internalization by cancer cells through receptor-mediated endocytosis [51] was investigated using the human breast cancer cell line MCF7. The TEM image of an ultrathin section (Fig. 5) shows an adherent PLGA-GNP particle to the surface of the cell and in the process of internalization into vesicles after 6 hour incubation with the cells (Fig. 5(a)). PLGA-GNP particle internalization inside a cytoplasmic vesicle is displayed in Fig. 5(b). The black dots are the GNPs (white arrows). The white areas are the hollow cores of the PLGA particles formed during the fixation process (orange dotted arrows). In these two TEM images, the GNPs are distributed along the inner surface of the PLGA shell. The reason is that during the cell specimen preparation, the cells were fixed with alcohols and resins. The PFH liquid was dried out and the GNPs were attached to the PLGA shell.

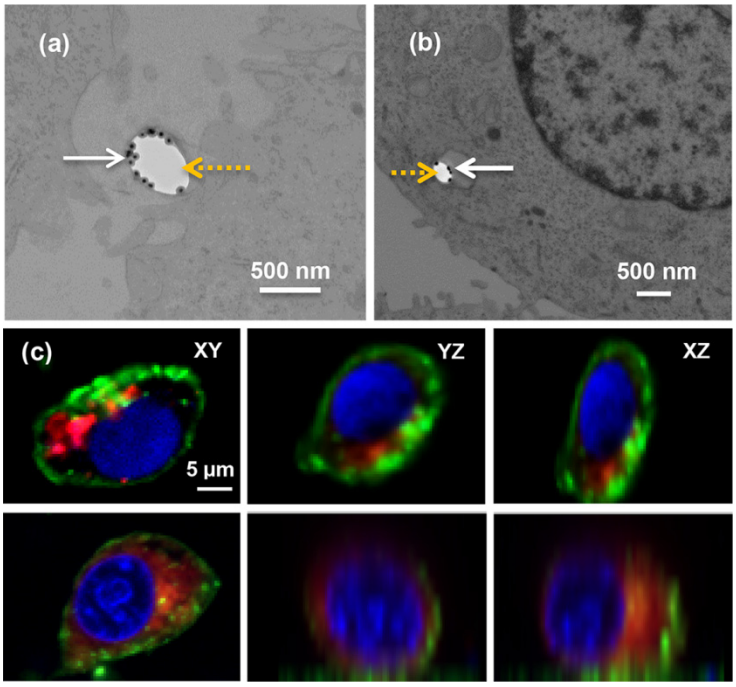

Fig. 5. (a)(b) TEM images of a single PLGA-GNP particle adherent to the surface of the cell and internalized in a cytoplasmic vesicle. The black dots are the GNPs (solid white arrows). The white areas are the hollow parts of the PLGA particles (dash yellow arrows). (c) Confocal laser scanning fluorescence images of PLGA-GNP particles uptake by MCF7 cells after 5-hour (top row) and 20-hour (bottom row) incubation. The images were cross sections at the centers of the cells at xy-, yz-, and xz- plane. The PLGA-GNP particles are labeled by DiI dye in red and are localized in the cell cytoplasm. The nuclei are stained blue by Hoechst. The cytoplasmic membranes are stained green by DiD dye. The scale bar is the same for all images.

Fluorescent images of MCF7 cells loaded with fluorescent dye DiI-labeled PLGA particles as a result of passive internalization are shown in Fig. 5(c). The images are the optical sections obtained at xy-, yz-, and xz- plane from cell center using a confocal laser scanning microscope. The cytoplasmic membranes are shown in green due to the fluorescent dye DiO stain; nuclei emit blue due to the Hoechst fluorescence; and DiI labeled PLGA-GNP particles are shown in red fluorescence. Top and bottom panels are MCF7 cells containing PLGA particles with 5 and 20 hours incubation time, respectively. Most of the PLGA-GNP particles are located in cellular endosomes after 5-hour incubation through a receptor-

Biomedical Optics EXPRESS

mediated endocytosis mechanism [51, 52], and are more dispersed in the cytoplasm after 20 hours incubation time.

3.4 PA/fluorescent imaging in vitro

The potential of PLGA particles as PA and fluorescent imaging contrast agents was investigated. The representative images of fixed MCF7 cells loaded with PLGA-GNP-DiI particles are shown in Fig. 6. The optical image was recorded using a 20x phase contrast objective (Fig. 6(a) and 6(d)). In the superimposed fluorescence images (Fig. 6(b) and 6(e)), the cell nuclei stained with Hoechst are shown in blue, the cytoplasmic membranes labeled with DiO are shown in green and the PLGA-GNPs labeled by DiI are shown in red and are located in the cytoplasm. In the PA images (Fig. 6(c) and 6(f)), a strong PA signal was observed at the location of the PLGA-GNPs. There is no PA signal at other parts of the cytoplasm, which is confirmed by the fluorescent image. These results confirm that the PLGA-GNP particles are excellent contrast agents for PA and fluorescent imaging in vitro. For the future in vivo experiments, since the fluorescence intensity decreases rapidly, the fluorescent contrast capacity could be used as assistance to PA imaging for shallow tissue imaging.

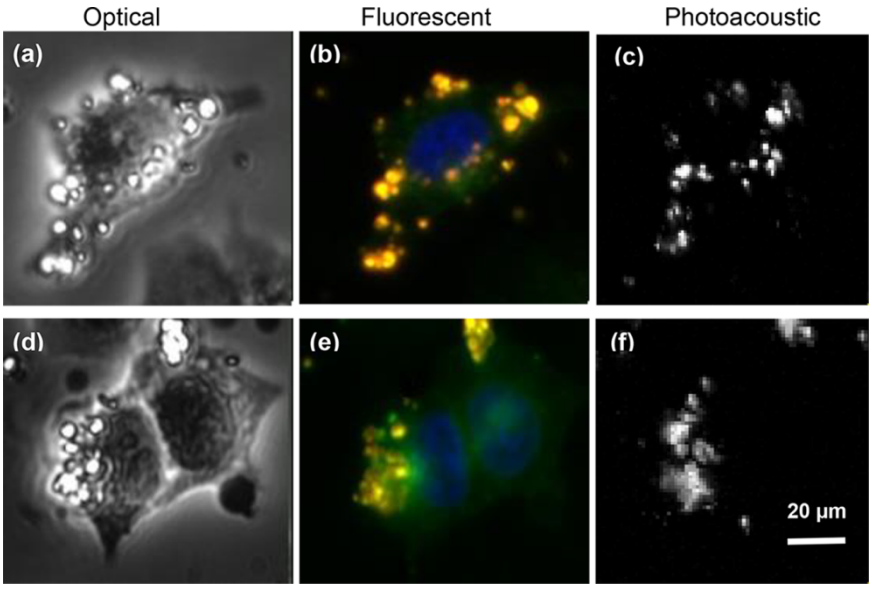

Fig. 6. Images of MCF7 cells loaded with DiI labeled PLGA-GNPs. (a)(d) The optical images were recorded using a 20x phase contrast objective. (b)(e) In the fluorescence images, the cell nuclei are shown in blue due to the Hoechst stain, and the cell membranes are shown in green by the DiO stain. (c)(f) The PA images were obtained using the 375 MHz transducer. The PLGA-GNPs particles are shown in yellow-orange in the fluorescence image (b)(e), and bright white in the PA image (c)(f). The scale bar is the same for all images.

3.5 PLGA particles as therapeutic agents

The effects of single PLGA-GNP particle vaporization inside the cells were investigated. Upon laser irradiation at fluence level of 100 mJ/cm^2, 1-2 μm sized PLGA-GNP particles vaporized within the cell as observed under optical microscopy. In some cases, the bubble remained trapped within the cell, slowly expanding over time and eventually escaped from the cell. Membrane integrity was lost upon bubble formation, and Propidium iodide (PI) fluorescence was observed within 20 seconds, indicating the membrane is damaged and the cell will die (Visualization 1 in the Supplementary Material). These results suggest that vaporization inside the cancer cells can cause mechanical damage to the cell which further

Biomedical Optics EXPRESS

causes cell death. The vaporization alone can serve as therapeutic purpose without drug assistance. This technique could be applied in an in vivo experiment. We are working on making smaller particles (mean size < 200 nm) for more effective tumor targeting in vivo. Even though the particles will be poly-dispersed, the larger size particles (< 500 nm) would be more sufficient at disrupting the vasculature, while the smaller particles would be more effective in penetrating deeper into the tumor upon successive treatments, and depositing PAC for localized drug delivery.

The chemo drug PAC loading efficiency by the PLGA particles was investigated using high performance liquid chromatography (HPLC) technique and it was quantified as 78.5% based on the ratio of amount of drug measured from sample particles to total amount of drug used for the synthesis. PLGA-GNP particle therapeutic capacities and PLGA particle drug delivery potential on a bigger cell population were tested. Immediately after the laser irradiation, the cell viability was tested using MTT assay, and test results are shown in Fig. 7(a). The exposure of PLGA-GNPs particles to the cells for 24 hours reduces the cell viability to 80%. The statistical analysis using a Student t-test shows that at a 95% confidence level, there is a significant difference between the control group and cell exposed to PLGA-GNP particles ($P < 0.05$). This result indicates a base level of cytotoxicity of the PLGA-GNP particle due to the large amount of PLGA-GNP particles used in the experiment. The cytotoxicity can be minimized by reducing the amount of the PLGA-GNPs for each treatment.

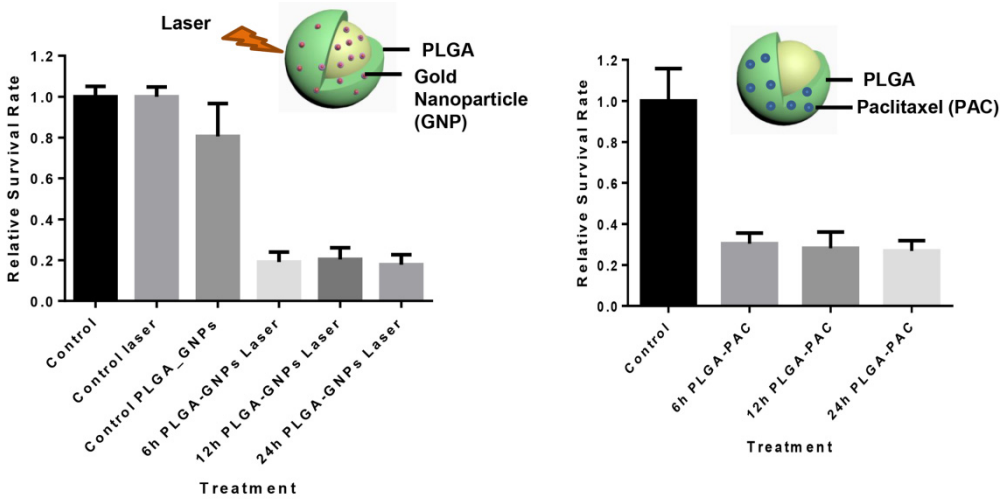

Fig. 7. (Left) MCF7 cells were exposed to PLGA-GNPs for 6, 12 and 24 hours. Then cells were irradiated with a 532 nm pulsed laser for 10 s/spot with a fluence of 100 mJ/cm^2. The cell viability was tested using MTT assay. (Right) MCF7 Cell viability after incubated with PLGA-PAC for 6, 12 and 24 hours was tested using a MTT assay. Error bars represent the standard deviation of 8 duplicates of each group.

After incubation PLGA-GNPs with MCF7 cell for 6, 12 and 24 hours, the laser induced vaporization reduces the cell viability to 19%, 20% and 18%, respectively. For cells exposed to PLGA-PAC particles for 6, 12 and 24 hours, the survival rates decreased to 30%, 28% and 27% respectively. The high cell survival rates induced by PAC might due to the insufficient amount of drug used in the experiment. The t-test results show that there are significant differences between the laser induced cell death and the paclitaxel induced cell death at a 95% confidence level ($P < 0.05$) for three incubation times. Overall, this result indicates that PAC was delivered to the cell via the PLGA particle released through a diffusion or erosion process. Laser induced vaporization demonstrates stronger therapeutic efficiency than using PAC. The combination of utilizing laser activation and drug release could achieve a better

Biomedical Optics EXPRESS

therapeutic efficacy with lower drug doses and reduced side effect in patients. The vaporization fluence used in this experiment was higher than the ANSI safety threshold. We will reduce the vaporization fluence in the future experiments by increasing GNP concentration and adjusting polymer composition (LA: GA ratio) in the shell to make the shell less rigid.

4. Conclusion

The main goal of this work was to synthesize and characterize nano-scaled, multi-model theranostic agents that worked simultaneously for combined PA and fluorescent imaging and drug delivery. The synthesis method provided a simple way to create contrast agents that is highly adaptable to specific applications in terms of particle size and types of GNPs encapsulation. In addition, knowing the contrast physical and PA properties will help us to optimize the experiment parameters for future studies. The phantom and in vitro studies showed strong PA signals using minimal light energy within the ANSI standards (< 20 mJ/cm^2) which indicates the potential of the PLGA-GNPs as PA contrast agents in clinical applications for shallow tissue image. If the optical absorbers are replaced by other types such as gold nanorods or gold nanoshells which absorb near infrared light, these agents primary uses could be for relatively deep tissue imaging. Beyond its contrast enhancing abilities, the agent therapeutic applications and drug delivery capacity to cancer cells were explored.

Funding

Canadian Institutes of Health Research (CCI-249368); Natural Sciences and Engineering Research Council of Canada; National Nature Science of China; Chongqing Medical University Innovation Team Plans (KJTD201303); Canada Foundation for Innovation; Ryerson University.

Acknowledgments

The authors thank Elizabeth Berndl for obtaining the confocal laser scanning fluorescent images, Dr. Krishan Sathiyamoorthy and Dr. Azhar Zam for assisting on the laser irradiation system setup.